Biophysical *Journal*
Article

Biophysical Society

Systematic measurements of interleaflet friction in supported bilayers

Autumn A. Anthony,[1] Osman Sahin,[2] Murat Kaya Yapici,[2] Daniel Rogers,[1] and Aurelia R. Honerkamp-Smith[1,*]
[1]Lehigh University, Bethlehem, Pennsylvania and [2]Sabanci University, Istanbul, Turkey

ABSTRACT When lipid membranes curve or are subjected to strong shear forces, the two apposed leaflets of the bilayer slide past each other. The drag that one leaflet creates on the other is quantified by the coefficient of interleaflet friction, *b*. Existing measurements of this coefficient range over several orders of magnitude, so we used a recently developed microfluidic technique to measure it systematically in supported lipid membranes. Fluid shear stress was used to force the top leaflet of a supported membrane to slide over the stationary lower leaflet. Here, we show that this technique yields a reproducible measurement of the friction coefficient and is sensitive enough to detect differences in friction between membranes made from saturated and unsaturated lipids. Adding cholesterol to saturated and unsaturated membranes increased interleaflet friction significantly. We also discovered that fluid shear stress can reversibly induce gel phase in supported lipid bilayers that are close to the gel-transition temperature.

SIGNIFICANCE This paper describes experiments in which shear flow is applied to supported membranes, causing the top leaflet of the membrane to slide over the lower one. The sliding velocity is limited by the friction between the two leaflets. Existing measurements and simulations of this friction coefficient have yielded a wide range of results. In our experiment, the interleaflet friction coefficient is independent of the flow rate, and we can measure different friction coefficients for membranes made from different lipid molecules. In addition, we show that flow induces a gel phase in supported membranes within a few degrees of their gel transition temperature.

INTRODUCTION

Plasma and internal membranes of living cells are formed from lipid bilayers. The mechanical properties of lipid membranes have been observed to direct membrane protein function and dynamics. Lipid-membrane composition modulates the opening probability of ion channels (1), and lipid-protein interactions modulate the clustering and activity of B cell receptors and glycosylphosphatidylinositol-anchored proteins (2,3). It is therefore not surprising that the complex lipid compositions found in living membranes are closely regulated (4). For this reason, the relationship between lipid-molecule structure and membrane properties such as viscosity, hydrophobic thickness, and intrinsic curvature are of interest to biophysicists.

Sliding of lipid monolayers past each other has been investigated in the context of boundary lubrication occurring in animal joints (5,6). The presence of phospholipids is required to achieve the low frictional coefficients observed at natural and artificial cartilage interfaces (7). However, it remains unclear how lipids are arranged at the cartilage surface and thus whether slip occurs between hydrophobic monolayer tails or hydrophilic head groups in multilamellar stacks (8). In addition, conflicting reports exist about whether lipids in the gel phase or liquid phase provide more efficient lubrication (6,9).

More generally, biological membranes take on large and small curvatures during events such as cell division, exo- and endocytosis, cell motility, and formation and growth of pilii or cilia. When membrane curvature changes, lipids in the inner and outer leaflets of the membrane must slide past each other. Pulling and translating membrane tubes or tethers from vesicles or cell membranes can also create significant interleaflet slip (10,11). This slipping motion is opposed by friction, characterized by the coefficient *b*. The magnitude of this coefficient helps determine the energy cost to deform membranes, as well as the speed with which deformations appear or dissipate. Accurate knowledge of this parameter

Submitted March 15, 2022, and accepted for publication June 22, 2022.
*Correspondence: auh216@lehigh.edu
Editor: Sarah L. Veatch.
https://doi.org/10.1016/j.bpj.2022.06.023

is required in order to correctly simulate biomembrane kinetics (12). It can also impact experimental measurements of other membrane properties, such as bending and compressiblity moduli.

The term interleaflet coupling is used to describe the interactions that arise from differences between the lipid composition of each leaflet. This coupling is frequently called λ or γ, and it acts to keep coexisting liquid domains in registry and to adjust the order parameter in each leaflet of single-phase asymmetric membranes (13,14). It may result from interactions at the tail regions of the lipids, in addition to membrane-spanning effects such as hydrophobic mismatch. In membranes with coexisting fluid domains, this parameter is defined as the free-energy cost of creating a misregistry of domains in the two membrane leaflets. Blosser et al. measured this parameter in supported membranes by measuring the force required to deregister domains that were initially in registry (15). In membranes surrounded by fluid, domains are always observed to be aligned to within the limits of optical resolution; in supported membranes, coupling between coexisting liquid domains in each leaflet depends strongly on the membrane and substrate-preparation techniques (16,17). This coupling is of interest in biological membranes because it has been shown to influence the phase behavior of asymmetric membranes (13,14,18). Several mechanisms for coupling have been identified, including acyl chain interdigitation, curvature coupling, lipid flip flop, and domain line tension (19).

In contrast, interleaflet friction occurs in all membranes regardless of their phase state or symmetry and is likely to result mainly from interactions at the contact region of the acyl tails. Interleaflet friction has been measured experimentally in model membranes. Estimates of the frictional coefficient have been determined from dynamics of pulling membrane tethers from giant vesicles (10,20), observations of vesicle shape fluctuations (21,22), diffusion of lipids in or vesicles adsorbed to supported lipid bilayers (23–25), and neutron-spin-echo measurements on bilayer stacks (26). Existing friction coefficients determined by the various methods span several orders of magnitude (see Table 1) and cannot be used to determine whether friction depends on lipid-molecule structure. In single-component membranes, some experiments find that diffusion in the upper and lower leaflets is tightly coupled (29,30), while others identify distinct diffusion constants in the upper and lower leaflets (31,32). Recent experiments and theoretical work (25,33) suggest that the coupling between the substrate and the lower leaflet of supported bilayers has a strong influence on lipid mobility in the upper leaflet. These results highlight the fact that mechanical properties of supported membranes are extremely sensitive to the details of their preparation.

Equilibrium and nonequilibrium simulations have been used to obtain systematic values of interleaflet friction. Using coarse-grained lipid models, den Otter and Shkulipa applied lateral shear to flat bilayers to investigate how length and asymmetry of the hydrocarbon tails contributed to the magnitude of the frictional coefficient (34). Their simulations showed that the frictional coefficient and likelihood of interdigitation of tails from each leaflet both increased with the degree of tail-length asymmetry. In membranes of symmetric lipids, interdigitation was negligible, but the frictional coefficient still increased slightly with tail length. This increase may reflect the larger variation in the position of tail ends or the closer spacing between the tail ends of the opposing leaflets. Zgorski, Pastor, and Lyman used a similar analysis of nonequilibrium steady-state shear response to identify how different force fields impact calculations of

TABLE 1 Selected experimentally determined values of interleaflet friction

Reference	Lipid(s)	b (Pa s/M)	Experimental method
Merkel et al., 1989 (23)	DOPC (18:1(Δ9-Cis) PC)	5×10^7–1.6×10^9	lipid diffusion in SLB by FRAP (10°C–45°C)
Blosser et al., 2015 (15)	DOPC	$5.2 \pm 0.4 \times 10^7$	shear-driven SLB tank treading
Tabaei et al., 2016 (24)	DOPC	$1.1 \pm 0.6 \pm 10^7$	particle tracking of vesicles adsorbed onto SLB
Schoch et al., 2018 (25)	DOPC	1.07×10^7	lipid diffusion in SLB by SPT
This work	DOPC	$4.59 \pm 0.28 \times 10^7$	shear-driven SLB tank treading
This work	DOPC + 30% cholesterol	$6.48 \pm 0.76 \times 10^7$	shear-driven SLB tank treading
Blosser et al., 2015 (15)	POPC (16:0/18:1 PC)	$5.8 \pm 0.8 \times 10^7$	shear-driven SLB tank treading
This work	POPC	$5.38 \pm 0.35 \times 10^7$	shear-driven SLB tank treading
Pott and Meleard, 2002 (22)	SOPC (18:0/18:1 PC)	2×10^8–5×10^9	dynamics of thermal shape fluctuations in vesicles
Evans and Yeung, 1994 (10)	SOPC, SM-chol	1×10^8	pulling tethers from vesicles
Jönsson et al., 2009 (27)	EggPC	2.4×10^7	shear-driven SLB tank treading
Schoch et al., 2018 (25)	EggPC	2.1×10^7	lipid diffusion in SLB by SPT
Bitbol et al., 2011 (21)	90:10 EggPC:brainPS	2–8×10^8	relaxation of pH-induced vesicle deformation
This work	DLPC (12:0 PC)	$5.50 \pm 0.80 \times 10^7$	shear-driven SLB tank treading
This work	DLPC + 30% cholesterol	$17.29 \pm 1.79 \times 10^7$	shear-driven SLB tank treading
Merkel et al., 1989 (23)	DMPC (14:0 PC)	2.7×10^7–2.9×10^9	lipid diffusion in SLB by FRAP (45°C)
Pfeiffer et al., 1993 (26)	DPPC (16:0 PC)	1×10^8	neutron spin echo in multilamellar stacks
Horner et al., 2013 (28)	DiphyPG (4ME 16:0 PG)	2.7–3.1×10^9	diffusion in black lipid membranes

Where temperature is not specified, it was described as room temperature and was likely to be between 22°C and 26°C. FRAP, fluorescence recovery after photobleaching; SPT, single-particle tracking.

friction in homogeneous bilayers of dipalmitoylphosphatidylcholine (DPPC) (35). They compared two versions of Martini and found that Martini 2.2 yielded 25% larger frictional coefficients than the older Martini 2004. Applying the same method to an atomistic CHARMM36 model required shorter time steps and therefore a shorter simulation. The strong attraction among the lipids in CHARMM required higher solvent shear rates to create steady traction forces and yielded a frictional coefficient approximately sixfold larger than that found by den Otter et al. The higher b values found using the atomistic simulation are similar to the range of values measured experimentally in DOPC-supported bilayers, differing by only a factor of two (see Table 2).

Recently, a new experimental method was invented that used microfluidic shear stress to cause "tank-treading," or sliding of the upper leaflet of a supported bilayer over the stationary lower one (Fig. 1) (27). Treating each membrane leaflet as a two-dimensional incompressible fluid sheet with the same viscosity, and assuming no-slip boundary conditions between the channel walls, the bulk fluid, and the upper membrane leaflet, Jönsson et al. solved two-dimensional Navier-Stokes equations for the two membrane sheets. The resulting expression includes frictional force between the substrate and the lower leaflet, frictional force between the two leaflets, shear forces and pressure gradients within the membrane sheets, and the shear force applied to the upper leaflet by the bulk flow. They concluded that the upper leaflet velocity is limited primarily by interleaflet friction; membrane viscosity makes a negligible contribution because membrane velocity changes only very gradually in the direction perpendicular to the flow. Similarly, using typical membrane compressibility moduli, they estimated that the influence of internal pressure gradients is also small (36). This method for measuring interleaflet friction has several advantages: it is geometrically and analytically simple, making results straightforward to interpret, it relies on observation of microscopic-scale movements of large continuous membranes, rather than single-particle tracking or nanometer-scale fluctuations, and it is independent of membrane curvature. In addition, Table 1 shows that the precision of this method relative to others is exceptionally high.

To determine how interleaflet friction depends on lipid-molecule structure, we require systematic measurements of interleaflet friction in bilayers made from different compositions using a consistent method. Here, we use the shear-stress-driven tank-treading method to determine interleaflet friction for multiple membrane compositions and determine how variations in lipid composition and fluorescent dye location influence the movement of the lipid bilayer. In addition, we report our observations of an apparent shear-flow-induced transition to the gel phase in bilayers near their main chain melting temperature. We are not aware of a previous description of this phenomenon.

MATERIALS AND METHODS

Chemicals

Lipids, including 1,2-dioleoyl-*sn*-glycero-3-phosphocholine (DOPC), 1-palmitoyl-2-oleoyl-glycero-3-phosphocholine (POPC), 1,2-dilauroyl-*sn*-glycero-3-phosphocholine (DLPC), and 1,2-dimyristoyl-*sn*-glycero-3-phosphocholine (DMPC) were obtained from Avanti Polar Lipids (Alabaster, AL, USA). Fluorescent lipids, including Texas Red 1,2-dihexadecanoyl-*sn*-glycero-3-phosphoethanolamine (TxRed DHPE), *N*-(4,4-difluoro-5,7-dimethyl-4-bora-3a,4a-diaza-*s*-indacene-3-propionyl)-1,2- dihexadecanoyl-*sn*-glycero-3-phosphoethanolamine (BODIPY DHPE), and 2-(4,4-difluoro-5-methyl-4-bora-3a,4a-diaza-*s*-indacene-3-dodecanoyl)-1-hexadecanoyl-*sn*-glycero-3-phosphocholine (BODIPY C12) were obtained from Invitrogen (Carlsbad, CA, USA). Calcium chloride was obtained from Biosciences (St. Louis, MO, USA), and all other chemicals were obtained from Sigma-Aldrich (St. Louis, MO, USA). Deionized (DI) water with conductance >18 MΩ/cm was obtained from a Millipore Direct-Q 3 UV system (Merck KGaA, Darmstadt, Germany).

Vesicle preparation

We made giant unilamellar vesicles by electroformation in 200 mM sucrose, as described previously (37). We produced large unilamellar vesicles by extruding giant unilamellar vesicles through a mini-extruder from Avanti Polar Lipids (Alabaster, AL, USA). The lipid sample was diluted in a high-salt buffer (HSB) of 100 mM NaCl, 10 mM Tris, and 1 mM EDTA at pH 8.0 and was pushed through a 0.1 μm filter in the extruder 19 times.

Channel preparation

We produced T-shaped polydimethylsiloxane (PDMS) microfluidic channels similar to those described previously (38), with cross-sectional dimensions 100 μm wide by 100 μm tall (Fig. 2 *A*).To prepare the microfluidic channels, first, replica molds were fabricated on silicon substrates using thick, epoxy-based, negative-tone permanent photoresist material. Specifically, the 50 μm-thick formulation of SU-8 (Kayaku Advanced Materials, Westborough, MA, USA) was used at low spin speeds to reach patterned

TABLE 2 Simulation-determined values of interleaflet friction

Reference	Lipid(s)	b (Pa s/M)	Simulation method
den Otter and Shkulipa, 2007 (34)	DOPC (18:1(Δ9-Cis) PC)	2.8×10^6	Martini
Zgorski et al., 2019 (35)	DOPC	$20.868 \pm 0.113 \times 10^6$	CHARMM36
den Otter and Shkulipa, 2007 (34)	DPPC (16:0 PC)	$2.4–3 \times 10^6$	Martini
Zgorski et al., 2019 (35)	DPPC	$11.282 \pm 0.034 \times 10^6$	CHARMM36
Zgorski et al., 2019 (35)	DPPC	$5.484 \pm 0.028 \times 10^6$	Martini 2.2
Zgorski et al., 2019 (35)	DPPC	$4.284 \pm 0.007 \times 10^6$	Martini 2004
Benazieb et al., 2021 (6)	DSPC (18:0 PC)	$2.54 \pm 0.1 \times 10^6$	Martini 2.0

Zgorski et al. measured all membranes at 10° above their chain melting temperature.

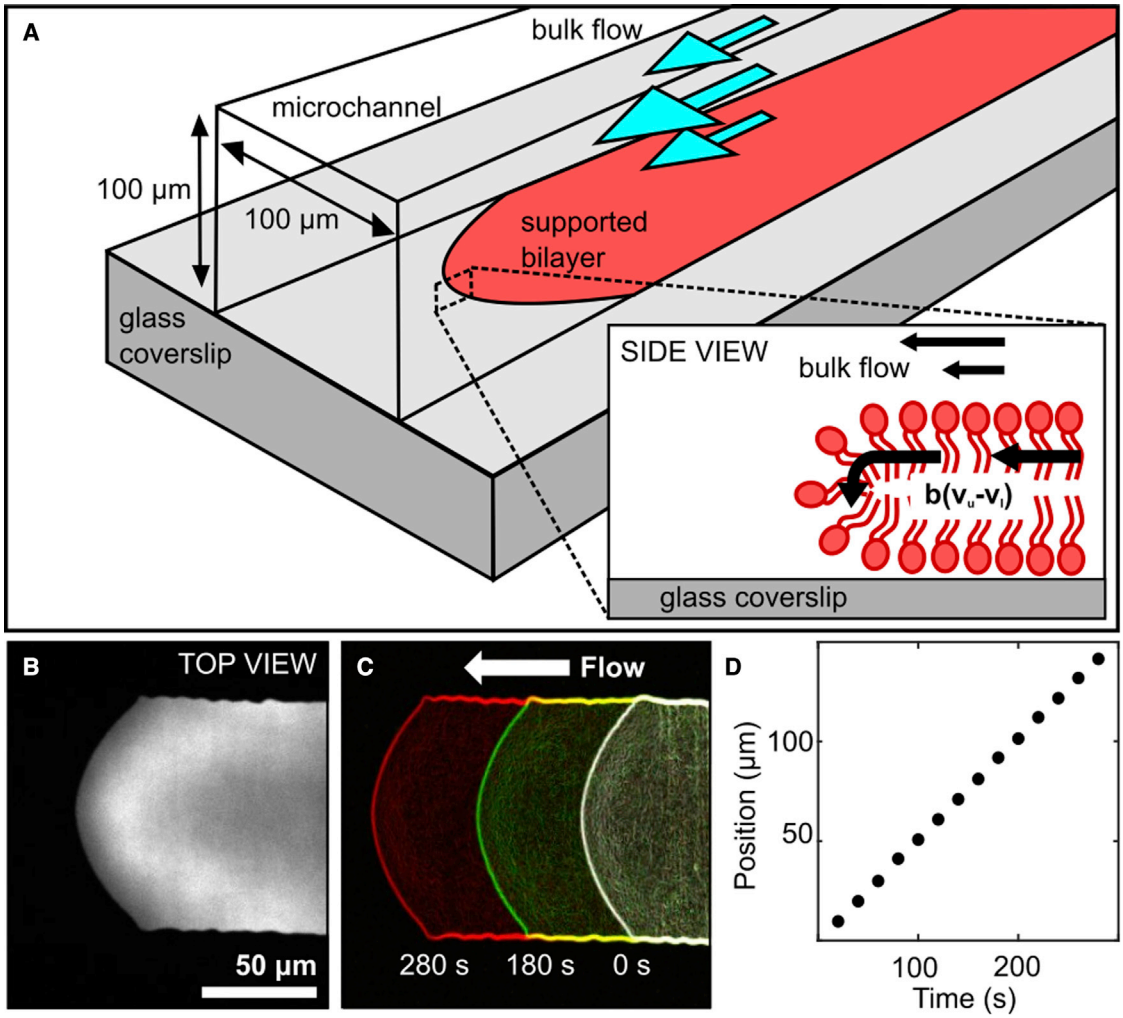

FIGURE 1 Microfluidic measurement of interleaflet friction. (*A*) Pressure-driven shear flow of the buffer causes the supported bilayer to tank tread along the microchannel. (*B*) The leading edge of a DOPC bilayer labeled with TxRed DHPE. (*C*) The bilayer leading edge, identified using edge detection in ImageJ, moves in the direction of flow (right to left) with constant velocity (*D*). To see this figure in color, go online.

SU-8 layer thickness in the range of 90–105 μm. The process started with dehydration of silicon wafers in a convection oven at 135°C for 5 min. After cooling down, SU-8 was poured directly onto the substrate surface, which was spin coated at 1000 Rpm for 30 s with an initial spread cycle of 10 s at 500 Rpm. Next, the sample was soft baked at 65°C for 10 min and 95°C for 30 min, followed by 365 nm ultraviolet (UV) exposure at a dose of 250 mJ. A two-step post-exposure bake was then performed at 65°C for 1 min and 95°C for 5 min. The sample was then immersed into SU-8 developer and agitated until patterns were clearly visible. Typically, the develop cycle took around 3 min and was completed by rinsing in isopropyl alcohol and blow drying with nitrogen. This optimized process yielded repeatable SU-8 patterns (Fig. 2 *B* and *C*) for molding the PDMS microchannels. Replicas were made using Sylgard 184 (DOW, Wiesbaden, Germany) and were cured at 60°C overnight before use.

Glass coverslips were treated to ensure they were flat and hydrophilic according to a previously published procedure (39). Briefly, rectangular coverslips (Corning, NY, USA) were sonicated in potassium hydroxide solution for 3 min and then rinsed extensively with DI water. They were then rinsed with ethanol, dried with nitrogen, and stored in a closed container. Immediately before each experiment, coverslips were cleaned with air plasma for 10 min. Both the coverslip and a PDMS channel were then plasma etched for 30 s then bonded together. After bonding, DI water was injected promptly to preserve the coverslip surface hydrophilicity. We note that our results were extremely sensitive to careful coverslip preparation.

Estimating shear force at the coverslip

Following a method used previously by Jönsson et al. (36), we determined the shear stress at the lower coverslip using the expression

$$\sigma = \frac{6\eta Q}{h^2(w - 0.630h)}\left[1 - \frac{8}{\pi^2}\sum_{n,odd}^{20}\frac{cosh(n\pi z/h)}{cosh(n\pi w/2h)}\right],$$

where η is the viscosity of the bulk liquid, Q is the flow rate, h is the channel height, w is the channel width, and z is the distance from the center line of the channel (in the direction perpendicular to flow). The shear-stress values provided in this paper are the average over all z. We note that this expression uses an approximation for the flow rate, Q, which is appropriate in the limit that the channel is wider than it is tall (40). Since our microchannel is square, this approximation underestimates flow rate by approximately 13%.

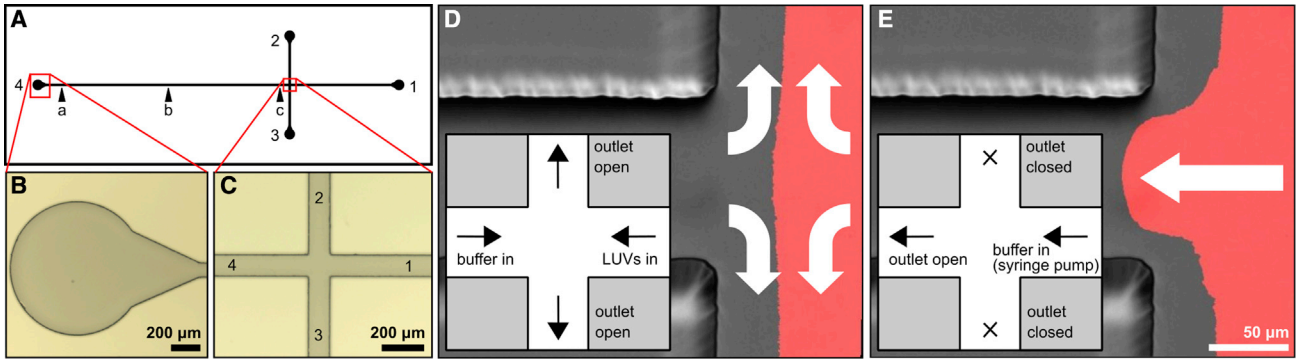

FIGURE 2 (*A–C*) The T-shaped channel design (*A*) was first created in 100 μm-thick SU-8 resin (*B* and *C*) then negatives were replicated in PDMS. (*D* and *E*) The supported bilayer was formed on the right-hand side of the channel by injecting both large unilamellar vesicles and buffer (*D*), followed by closing ports 2 and 3 and using flow to drive the supported bilayer toward port 4 (*E*). The leading edge of the bilayer was imaged while moving between the location indicated by arrow (*c*) toward arrows (*b*) and (*a*). To see this figure in color, go online.

We determined the dimensions of our PDMS microchannels by measuring multiple cross sections within each one and determined that the average channel cross section was 100 ± 11 μm in height and 96 ± 1.9 μm in width. Using these measured standard deviations, we estimated uncertainty in the applied shear force at each flow rate and the uncertainty in the friction value *b*. Variations in the measured bilayer velocity were much smaller (approximately 1%), so these were neglected. In square microchannels, we expect PDMS expansion due to pressure to be minimal (41).

Bilayer formation

All equipment and flow buffer were allowed to equilibrate to room temperature, which, in our laboratory, was between 27°C and 28°C, before experiments started. Supported lipid bilayers were formed in the right side of a T-shaped channel. Large unilamellar vesicles were diluted in HSB with 10 mM calcium chloride to speed vesicle fusion and flowed into outlet 1 of the channel. Simultaneously, HSB was flowed into outlet 4 of the channel at the same rate, allowing the buffer and vesicles to meet in the middle, with excess solution flowing out of outlets 2 and 3 (Fig. 2 *D*). This formed a bilayer only on the right side of the channel, with a flat edge in the middle of the intersection. After the bilayer formed, the vesicle tube was removed, and EDTA-containing flow buffer was allowed to flow through outlet 1 to flush out any remaining vesicles and calcium. Then, a tube connected to a syringe pump was inserted into outlet 1, valves connected to outlets 2 and 3 were closed, and outlet 4 was connected to the waste container. After flow was applied, the bilayer began to tank tread along the channel toward outlet 4 (Fig. 2 *E*). Once the bilayer entered the long arm of the T and the front edge reached a steady-state shape, fluorescence movies were recorded.

Image analysis

Microscopy was performed with a 20× objective on a spinning disk confocal microscope (Intelligent Imaging Innovations, Denver, CO, USA). Five-min-long time-lapse movies were recorded at one frame every 20 s for 30 min. All image analysis was performed using ImageJ (42). The "Find Edges" function was first used to identify the bilayer edge (Fig. 1 *C*). A line was then drawn horizontally through the center of the channel to locate the position of the leading edge using the "Find Peaks" plugin. This was then used to track the position of the leading edge over the time of the movie, yielding a tank-treading velocity *v* (Fig. 1 *D*). In some cases, the images were first smoothed using the "Median" filter with a radius of 10 pixels and then thresholded before using the Find Edges function.

Measuring interleaflet friction

We calculated the average shear stress at the coverslip surface σ and interleaflet friction *b* as done previously by Jönsson et al. (43). After forming each bilayer in an individual microchannel, it was subjected to a single flow rate. An approximately 10 min period was allowed for the membrane to enter and fill the longer leg of the T channel (between points c and a in Fig. 2 *A*) and for the leading-edge shape to reach a steady state before recording was started. To validate the method and check that membrane response was linear, we flowed buffer through channels at rates of 0.2, 0.3, and 0.4 mL/min. Surface shear stress varies with proximity to the channel edge, so we report the average value of σ calculated for each flow rate: 24.8 ± 1.4, 37.7 ± 4.2, and 51.5 ± 5.5 Pa, respectively. Note that surface shear stress σ has the same units, Pa, as pressure (discussed later). We chose the lower flow rate because it resulted in convenient membrane leading-edge velocities for measurement; previous experiments show that membranes undergo tank treading whenever shear stress is larger than about 3–5 Pa. Flow rates larger than 0.8 mL/min caused a large pressure build up in the channel, resulting in leaks. We measured velocity in 3 different channels per flow rate, yielding 9 independent measurements of friction for each lipid composition (Fig. 3). Previous results showed that in a similar microfluidic channel and with applied shear force, the lower leaflet remained stationary, and that velocity of the bilayer front was half the velocity of the upper leaflet (43). Using the observed velocity and calculated surface shear stress, we calculate the average coefficient of interleaflet friction $b = \frac{\sigma}{2v}$ for each experiment. The average and standard deviation for 9 measurements of each different membrane composition are reported in Figs. 4 and 6.

RESULTS

Fluorescent lipids

The tank-treading method requires that we include a fluorescent lipid to visualize the leading edge of the bilayer. Therefore, we first investigated whether the presence of fluorescent lipids would impact our results by measuring friction in DOPC bilayers containing 0.8 mol % of either TxRed DHPE, BODIPY DHPE, or BODIPY C12 (Fig. 4). We obtained similar results for the head-labeled lipids: $4.59 \pm 0.28 \times 10^7$ Pa s/m for membranes labeled with TxRed DHPE, and $4.21 \pm 0.52 \times 10^7$ Pa s/m for membranes labeled with BODIPY DHPE. While the difference

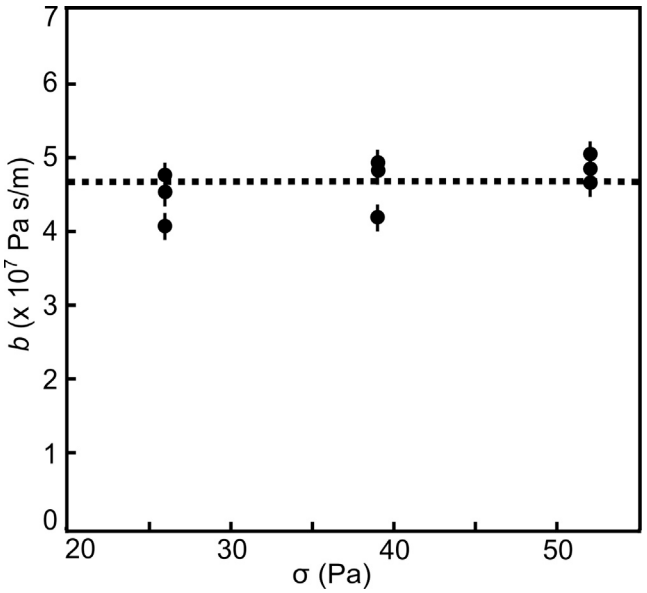

FIGURE 3 We measured the coefficient of interleaflet friction b in DOPC bilayers in nine independent trials using three different flow rates. Results are plotted versus the average shear stress at the lower coverslip, σ. Error bars indicate the estimated uncertainty for each friction measurement due to variation in microfluidic channel height. Measured friction values do not show a strong trend with shear stress over the range that we investigated.

between the two head-labeled lipids was smaller than the measurement uncertainty, including the tail-labeled lipid BODIPY C12 reduced the measured friction by about 17%, yielding $3.82 \pm 0.43 \times 10^7$ Pa s/m. Fluorophore structure also dramatically affected the distribution of lipid dye at the moving bilayer front. Concentrations of TxRed DHPE and BODIPY DHPE peaked 20–30 μm behind the bilayer leading edge (Fig. 5). In contrast, the fluorescence of BODIPY C12 increased roughly linearly for several hundred micrometers behind the edge before leveling off to a constant value. These observations are consistent with those reported previously (27). All three fluorophores were distributed homogeneously over the membrane several minutes after flow was stopped (data not shown).

Lipid structure

We next measured friction in five different membrane compositions, using 0.8 mol % TxRed DHPE to label each (Fig. 6 *A*). First, we compared a doubly unsaturated lipid, DOPC, with POPC and measured $4.59 \pm 0.28 \times 10^7$ and $5.38 \pm 0.35 \times 10^7$ Pa s/m, respectively (Fig. 6 *B*). These values are very similar to those obtained by Blosser et al. using the same method, including the observation that friction in POPC membranes is slightly higher than that in DOPC. In order to measure friction in a saturated bilayer, we chose DLPC, which has two saturated 12-carbon chains and a melting temperature of −2°C, to ensure that the membrane would be in a fluid state. DLPC membranes had interleaflet friction $5.50 \pm 0.80 \times 10^7$ Pa s/m, similar to POPC.

Finally, we investigated the impact of cholesterol on interleaflet friction. Adding 30 mol % cholesterol to DOPC yielded a 40% increase in friction, to $6.48 \pm 0.76 \times 10^7$ Pa s/m. Adding 30 mol % cholesterol to DLPC resulted in an even larger increase, approximately 215%, to $17.29 \pm 1.8 \times 10^7$ (Fig. 6 *C*). This large increase in friction meant that higher flow rates (0.4 and 0.8 mL/min or 51.5 ± 5.5 and 103.1 ± 11 Pa) were required to observe the bilayer velocity, which led to frequent device failures. For this reason, the DLPC + cholesterol measurement is the average of only four trials at two flow rates.

Flow-induced lipid phase transition

DMPC has two saturated 14-carbon tails and a gel-transition temperature of 24°C. We produced a supported bilayer of DMPC as described earlier and confirmed it was fluid at our laboratory room temperature (27°C) using fluorescence recovery after photobleaching. However, when we applied high shear stress to initiate tank treading, we instead observed that the membrane in the center of the channel darkened significantly, and little to no movement of the bilayer front was observed. We determined using fluorescence recovery after photobleaching (FRAP) that

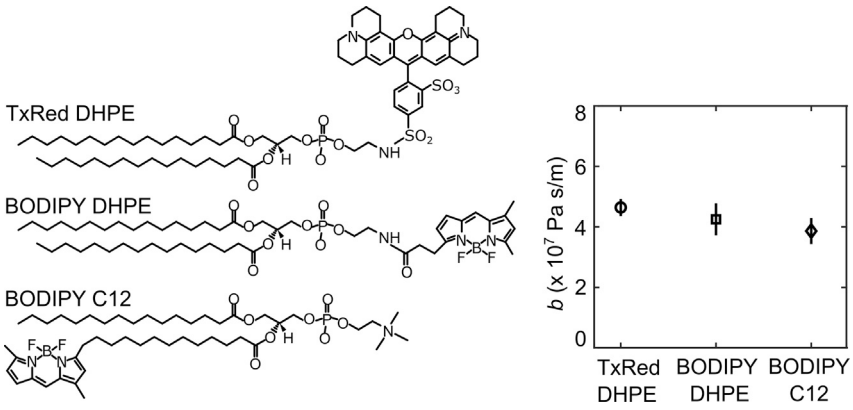

FIGURE 4 Left: structures of the fluorescent lipids used in this study. Right: measured values for the coefficient of interleaflet friction DOPC bilayers containing 0.8 mol % of each fluorescent dye. Values are the average of nine measurements and error bars show one standard deviation.

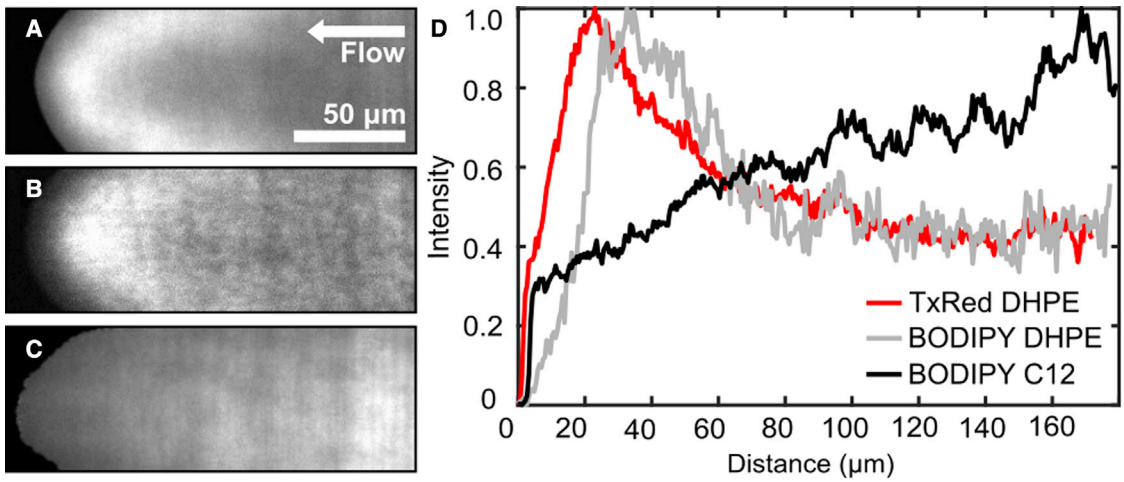

FIGURE 5 Fluorescent dye distributions in tank-treading DOPC membranes. (*A–C*) TxRed DHPE (*A*) and BODIPY DHPE (*B*) peak behind the membrane leading edge, while BODIPY C12 fluorescence (*C*) is depleted near the edge. Profiles of normalized intensity along the center of the bilayer are shown in (*D*), with the bilayer front edge position set to zero. To see this figure in color, go online.

fluorescence recovery times in the darkened region increased significantly (Fig. 7 *A–C*). After flow was stopped, fluorescence in the center region gradually increased, and FRAP recovery times returned to their original values (see Fig. 7 *D* and *E* and Video S1). We explain these observations by hypothesizing that the membrane enters a shear-stress-induced gel phase. The loss of fluorescence signal observed in the central region could be the result of TxRed DHPE being excluded from the gel phase or of self-quenching due to change in intermolecular spacing.

The width of the dark region is also sensitive to pressure. We observe a wider dark region near the inlet of the channel, where pressure is high, than near the outlet (Fig. 8 *A–C*). We estimate that the pressure difference between these two locations is ≈428 Pa at a flow rate of 0.005 mL/min, while shear stress does not vary along the length of the channel. The width of the dark region increases at higher flow rates (Fig. 8 *D–F*).

DISCUSSION

Consistent with previous experimental (15,36) and simulation (34,35) results, we observe that b is independent of shear stress over the range we probed. The tank-treading method has the advantages that it probes friction using steady-state, micron-scale membrane motion and that data

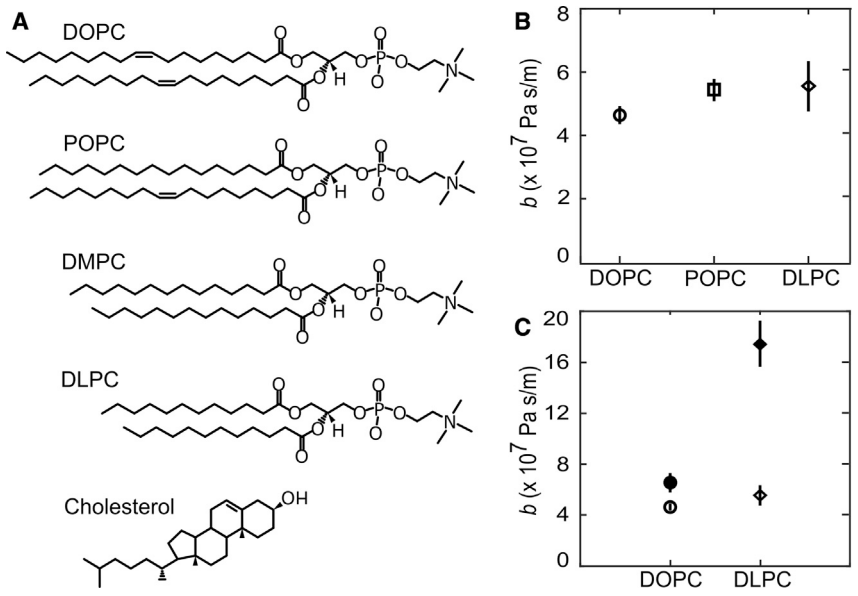

FIGURE 6 (*A*) Chemical structures of the lipids used in this experiment. (*B*) Measured values of coefficients of interleaflet friction for DOPC, POPC, and DLPC. (*C*) Coefficients of interleaflet friction for DOPC and DLPC with 0 (*open markers*) and 30% (*solid markers*) cholesterol with 0.8 mol % TxRed DHPE. With the exception of DLPC, values shown are averages over at least 9 measurements at 3 different flow rates; error bars are one standard deviation wide. We were not able to determine a friction coefficient for DMPC.

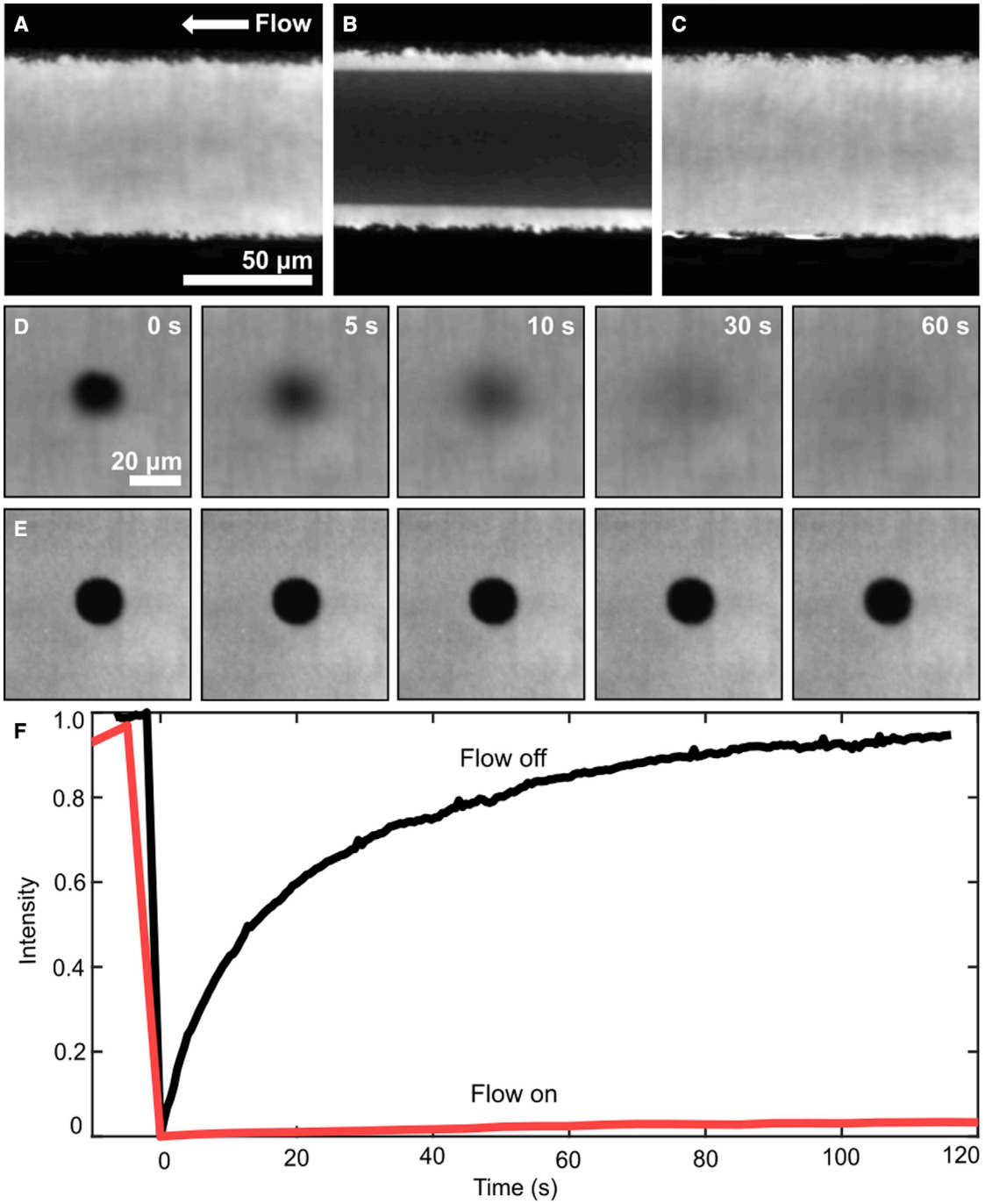

FIGURE 7 (*A*) DMPC bilayer before flow is applied. (*B*) Bilayer during a flow of 0.005 mL/min (0.64 Pa). The brighter edges of the bilayer remain fluid. At this low shear stress, the bilayer is unlikely to be tank treading. Images were recorded at approximately position (*b*) as indicated in Fig. 2 *A* after depositing large unilamellar vesicles in the left-hand arm of the channel instead of the right-hand one. (*C*) Fluorescence intensity recovers to its former value about 10 min after stopping flow. (*D* and *E*) FRAP images of a DMPC bilayer (*D*) before and (*E*) during flow. To improve visibility, we adjusted contrast of images in (*E*) to match those in (*D*) and matched contrast for images (*A*)–(*C*). (*F*) FRAP recovery time increased sharply with flow on. To see this figure in color, go online.

interpretation is straightforward. Since during the tank-treading method the lower leaflet is continually produced directly from the upper leaflet lipids, we believe that membrane asymmetry is minimized. The major sources of uncertainty in our measurements include variation in microfluidic device dimensions and variation in preparation of the glass substrate. Despite this variation, we observed distinct frictional coefficients in membranes with different compositions. This method's versatility could be further improved with modifications to the experimental procedure.

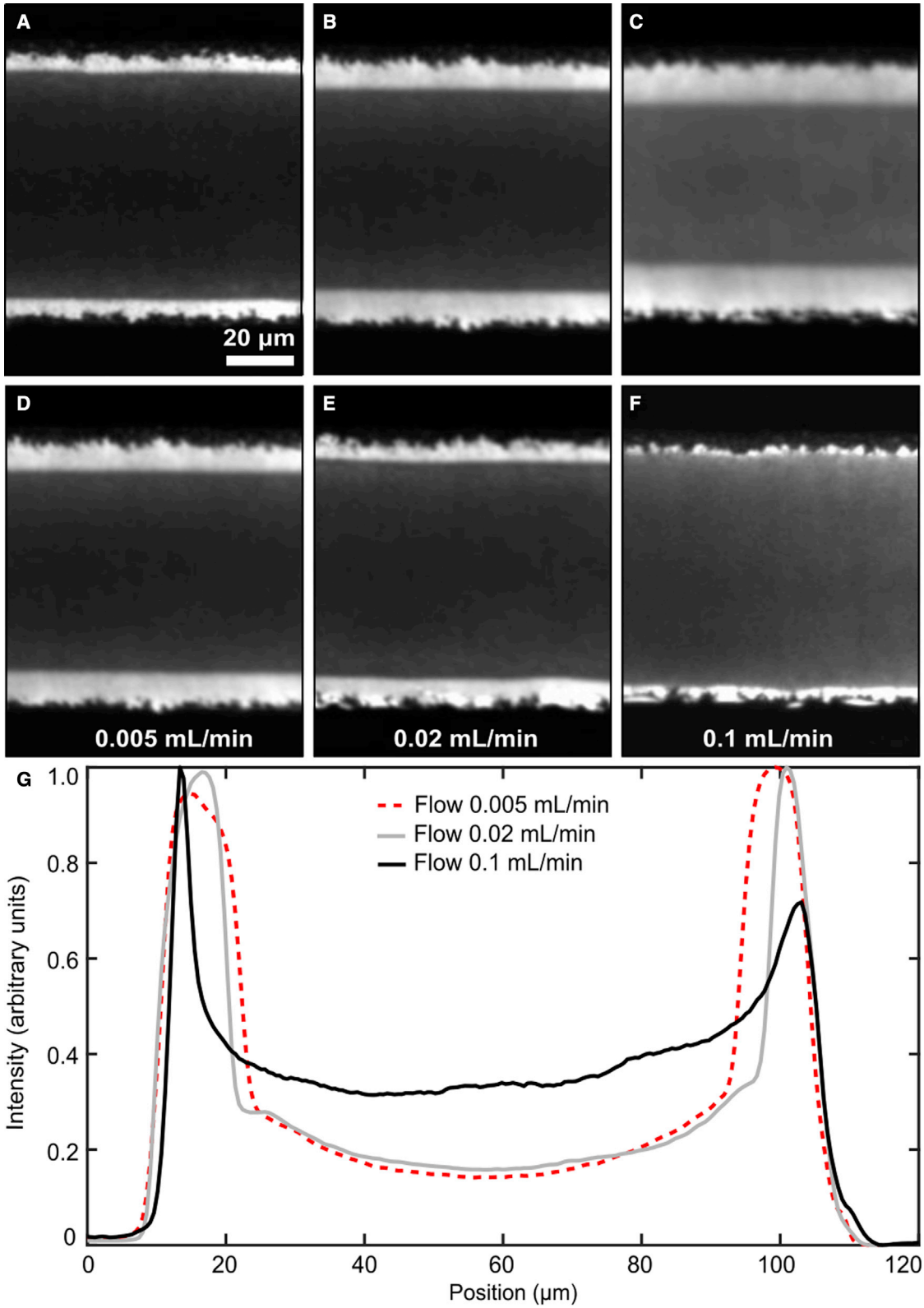

FIGURE 8 The width of the gel region depends on the fluid pressure in the channel as well as on the magnitude of the shear stress. (*A–C*) Images are shown near the inlet (*A*), center (*B*), and outlet (*C*) of the same channel at a single flow rate (0.005 mL/min). Images in (*A*), (*B*), and (*C*) were recorded close to the locations (*a*), (*b*), and (*c*), as indicated in Fig. 2 *A*, respectively (flow direction was reversed in this experiment). (*D*)–(*F*) show the central region of the channel (near location *b*) at three different flow rates, which forms a wider gel phase region in the center. (*G*) shows the intensity averaged along the channel length for the same flow rates shown in (*D*)–(*F*). Image contrast in all panels, and intensities shown in (*G*), were normalized to the brightest region in the image. To see this figure in color, go online.

Temperature

Shear-driven membrane tank treading only occurs in fluid-phase membranes. The most serious limitation to the experiments described here was the lack of temperature control, which constrained the lipids that could be investigated to those with chain melting temperatures significantly below room temperature. Applying high shear stress creates a technical challenge since the temperature of both the substrate and the flowing liquid should be controlled. We plan to implement temperature control in future experiments so that we can determine how b changes with temperature, measure friction in a wider variety of lipid mixtures, and more precisely match the conditions used in simulation experiments. For instance, Zgorski et al. set temperature at a constant 10°C above the gel-transition temperature for that lipid. This means that the friction we measured in DLPC and DOPC at the same temperature, 27°C, cannot be directly compared with the simulation results.

While absolute values of b differ significantly between the simulations of Zgorski et al. and den Otter and Shkulipa, they are consistent with the finding that interdigitation between tails in opposing leaflets increases interleaflet friction. Zgorski et al. find that the coefficient for DOPC is about twice that of DPPC because of an increase in tail overlap in the DOPC bilayer. In our experiment, while we cannot directly compare DLPC and DOPC, we can compare DLPC with POPC since their transition temperatures are similar. Considering only the likelihood of interdigitation, we might expect that the value measured in POPC would be higher than that in DLPC. Instead, we find that they are almost identical. However, this may be due to other differences between DLPC and POPC membranes. Comparison of the friction in membranes made from lipids that are both saturated and asymmetrical, and with differing degrees of asymmetry, would more specifically address this question.

Including 30% cholesterol caused a significant increase to interleaflet friction in DOPC membranes but an even more dramatic increase in DLPC bilayers. This result is consistent with an observation by Marquardt et al.: DLPC has shorter acyl chains, so the bilayer is thinner; neutron diffraction and scattering data suggest that this forces cholesterol to span the midplane of DLPC membranes (44). This explanation predicts that a less dramatic increase would be observed in DPPC bilayers on adding cholesterol. Further insight could be gained by incorporating membrane-spanning proteins or peptides.

Pressure

Significant shear stress (25–50 Pa) is required to cause membrane tank treading, which we accomplish by using a small channel (100 by 100 μm) and high flow rates. At the flow rates used in this experiment, we estimate that the pressure drop in the longer leg of the T ranges from 1.7×10^4 to 4.2×10^4 Pa (along the length of the channel, pressure decreases linearly with distance from the inlet) (45). While it is possible that pressure alters the interleaflet friction coefficient, we did not observe a significant change in friction over an approximately twofold pressure increase for the same lipid. In Fig. 3, the estimated pressure in the channel increased from 2.6×10^4 Pa at the lowest flow rate, to 3.4×10^4 Pa at the middle one, up to 4.3×10^4 Pa at the highest flow rate. Future microfluidic devices will be redesigned to further decouple pressure and shear stress, in addition to enabling temperature control.

Fluorescent labels

Our membranes include fluorescent lipids so that we can observe the translation of the supported bilayer. We found that even with less than 1 mol % label, the choice of fluorescent label affected the measured value. In particular, including a tail-labeled fluorescent lipid reduced the observed friction. This is consistent with previous observations (27) and may indicate that the label causes disruption of lipid tail packing in the hydrophobic region at the bilayer center or that it facilitates photoxidation of unsaturated lipids. This perturbation could be reduced by lowering the concentration of fluorescent label or by using a label-free microscopy method compatible with applying significant fluid shear.

Our observation of fluorescent lipid distribution within tank-treading bilayers is consistent with previous observations by Jönsson et al. Briefly, they observed that lipids with a head-group-located fluorophore were located mostly in the upper leaflet of the bilayer and that they accumulated near the leading edge of the membrane during tank treading. They concluded that labeled lipids are sterically excluded from the newly formed lower leaflet as the bilayer edge rolls over. Conversely, fluorophores located in the tail region of the bilayer were present in both leaflets and observed two distinct drift velocities. FRAP experiments indicated that upper leaflet dye moved at a similar velocity to the surrounding lipids. However, lower leaflet dye, instead of being stationary, moved forward at 10% of the velocity of the leading edge, due to coupling with the molecules in the upper leaflet. On average, tail-labeled dye molecules were depleted from the leading edge, explaining the linear concentration gradient that we also observed (27). The same authors have also published detailed calculations of the forces and internal pressure gradients acting on molecules in tank-treading bilayers, including the impact of accumulation of labeled molecules at the leading edge (43,46).

Some authors speculate that friction in supported bilayers may be intrinsically different to that in vesicles or unsupported membranes due to the change in lipid dynamics near a solid surface (6). For example, lipid-diffusion constants and gel-transition temperatures are observed to shift

when supported and fluid-surrounded membranes are compared (29,47,48). Table 1 shows that experimental measurements of friction in vesicles or black lipid membranes tend to yield larger estimates for b than measurements in supported bilayers (with a few exceptions). However, only a few measurements in vesicles exist, and several of the estimates in both systems span large ranges. It is not clear whether these measurements reflect an actual difference in interleaflet friction between these systems or simply result from use of different experimental methods and analytical assumptions. This could be resolved by more systematic measurements of friction in unsupported membranes.

Flow-induced gel phase

Our observation of flow-dependent gel-phase formation was unexpected. Zgorski et al. found that membranes exhibit shear thinning at high shear rates (35). Similarly, some experiments show that viscosity of living plasma membranes is reversibly lowered by shear stress (49,50). Shear-thickening fluids are less common than shear-thinning ones, but flow-induced crystallization occurs in some high molecular weight polymer solutions (51) as well as in colloidal solutions.

In unsupported membranes, pressure increases lipid miscibility and gel-transition temperatures, increasing gel-transition temperatures by 22°C per kbar in saturated lipids such as DPPC and DMPC (52). The pressure required to increase the transition temperature of DMPC by 3°C would be 0.1364 kbar or 1.36×10^7 Pa, much larger than that applied in our experiment. Therefore, although we observe that the DMPC phase transition is sensitive to pressure (Fig. 8), it cannot be explained solely by a pressure increase. Another indication that shear stress, rather than pressure, is responsible for forming the gel phase we observe is the spatial patterning of the gel. At a given location within the channel, gel phase forms in the center, while the edges remain fluid. After flow starts, the gel appears first in the center and broadens to its steady-state width, while after the flow stops, the gel appears to melt from the outside edges in (see Videos S1 and S2). While pressure is the same at all locations within the channel at a given distance along its length, shear stress at the lower coverslip is largest in the center of the channel and diminishes to zero at the upper and lower edges. From the images, we can infer that the threshold shear stress required to induce gel phase in Fig. 7 *B* is 0.13 Pa. In contrast to the high shear stress required to induce tank treading, the gel phase appears at lower shear stress, well within the range experienced by living cells in a variety of contexts; for example, the shear stress experienced by endothelial cells due to blood flow is generally approximated as 1.5 Pa.

For single-component membranes, the liquid-gel transition is generally observed to shift to higher temperatures, and occur over a broader temperature range, in supported membranes compared with unsupported ones (53). Charrier and Thibaudau observed that DMPC bilayers supported on mica exhibited two distinct phase transitions, one occurring between 28°C and 33°C and the other between 39°C and 45°C, which they attributed to distinct phase transitions occurring in each leaflet (47). Our previous work showed that the apparent liquid-liquid miscibility temperature of ternary lipid mixtures increases by 2°C to 10°C in supported membranes compared with those measured in vesicles (48). The magnitude of the temperature shift, and the coupling between upper and lower leaflets, depend on the details of the substrate and sample preparation. However, these prior observations suggest that the gel-transition temperature in our DMPC membranes may be shifted up to just below 27°C or that sub-micron-sized gel domains may be present within the DMPC bilayer. This could help nucleate formation of gel phase when shear stress is applied.

Tension, lateral pressure, and tilt

Theory and experiments confirm that applying lateral tension to vesicles reduces liquid-liquid miscibility temperatures (54,55). In two-component vesicles, applying ~3 mN/m of membrane tension reduced the gel-transition temperature by 1°C, and applied tension determined whether tilt or ripple gel phase formed (56). Applying a lateral pressure to the membrane can be expected to have the opposite effect, increasing the gel-transition temperature. It is plausible that applying lateral shear flow to a supported membrane creates effective, heterogeneous lateral pressure on small regions of the membrane between pinning sites, allowing the membrane to enter a gel phase. However, it is difficult to estimate the value of applied pressure due to the heterogeneity of the membrane-surface coupling. We plan to continue investigating the properties of the shear-induced gel phase in future experiments.

Here, we show that the shear-driven tank-treading bilayer method yields consistent values for b at different flow rates and is sensitive enough to identify distinct coefficients of interleaflet friction in membranes made from different lipids. This makes it possible to systematically explore this parameter in lipid-composition space for the first time, with greater precision than has previously been achieved. More explicit measurements of this fundamental parameter have the potential to improve our understanding of membrane mechanics. For example, assumptions about the strength of interleaflet coupling are required in order to determine how the membrane bending modulus depends on lipid composition via multiple techniques (57–60). Our observation of a significant increase in interleaflet friction when cholesterol is added to DOPC may impact interpretation of these experimental results. Incorporating temperature control will expand the range of lipids and lipid mixtures that can be studied using this method. Additional careful measurements of friction in membranes will generate insight into the mechanism of interleaflet coupling and into the origin of existing discrepancies between simulated and measured values.

SUPPORTING MATERIAL

Supporting material can be found online at https://doi.org/10.1016/j.bpj.2022.06.023.

AUTHOR CONTRIBUTIONS

A.A.A. and A.R.H.-S. designed the research. A.A.A. and D.R. carried out experiments. A.A.A. analyzed the data. O.S. and M.K.Y. manufactured master molds for microfluidic channels. A.A.A. and A.R.H.-S. wrote the article.

ACKNOWLEDGMENTS

The authors thank Dr. Sreeja Sasidharan for helpful discussions and for assistance with experiments and with calculations. We also thank John Gregoris for fabrication of scientific apparatus. A.A.A. was supported by a New Initiative Grant from the Charles E. Kaufman Foundation.

DECLARATION OF INTERESTS

The authors declare no competing interests.

REFERENCES

1. Keller, S., S. Bezrukov, …, V. Parsegian. 1993. Probability of alamethicin conductance states varies with nonlamellar tendency of bilayer phospholipids. *Biophys. J.* 65:23–27. https://doi.org/10.1016/s0006-3495(93)81040-3. https://linkinghub.elsevier.com/retrieve/pii/S0006349593810403.

2. Stone, M. B., S. A. Shelby, …, S. L. Veatch. 2017. Protein sorting by lipid phase-like domains supports emergent signaling function in B lymphocyte plasma membranes. *eLife.* 6:e19891. https://doi.org/10.7554/elife.19891. https://elifesciences.org/articles/19891.

3. Raghupathy, R., A. A. Anilkumar, …, S. Mayor. 2015. Transbilayer lipid interactions mediate nanoclustering of lipid-anchored proteins. *Cell.* 161:581–594. https://doi.org/10.1016/j.cell.2015.03.048. https://linkinghub.elsevier.com/retrieve/pii/S0092867415003682.

4. Levental, K. R., E. Malmberg, …, I. Levental. 2020. Lipidomic and biophysical homeostasis of mammalian membranes counteracts dietary lipid perturbations to maintain cellular fitness. *Nat. Commun.* 11:1339. https://doi.org/10.1038/s41467-020-15203-1. http://www.nature.com/articles/s41467-020-15203-1.

5. Falk, K., N. Fillot, …, C. Loison. 2014. Interleaflet sliding in lipidic bilayers under shear flow: comparison of the gel and fluid phases using reversed non-equilibrium molecular dynamics simulations. *Phys. Chem. Chem. Phys.* 16:2154–2166. https://doi.org/10.1039/c3cp53238k. http://xlink.rsc.org/?DOI=C3CP53238K.

6. Benazieb, O., C. Loison, and F. Thalmann. 2021. Rheology of sliding leaflets in coarse-grained DSPC lipid bilayers. *Phys. Rev. E.* 104:054802. https://link.aps.org/doi/10.1103/PhysRevE.104.054802.

7. Yuan, H., H.-W. Cheng, …, M. Valtiner. 2021. Lipid anchoring improves lubrication and wear resistance of the collagen I matrix. *Langmuir.* 37:13810–13815. https://pubs.acs.org/doi/10.1021/acs.langmuir.1c01581.

8. Lin, W., and J. Klein. 2021. Recent progress in cartilage lubrication. *Adv. Mater.* 33:2005513. https://onlinelibrary.wiley.com/doi/10.1002/adma.202005513.

9. Wang, M., T. Zander, …, A. Dėdinaitė. 2015. The effect of temperature on supported dipalmitoylphosphatidylcholine (DPPC) bilayers: structure and lubrication performance. *J. Colloid Interface Sci.* 445:84–92. https://doi.org/10.1016/j.jcis.2014.12.042. https://linkinghub.elsevier.com/retrieve/pii/S0021979714009953.

10. Evans, E., and A. Yeung. 1994. Hidden dynamics in rapid changes of bilayer shape. *Chem. Phys. Lipids.* 73:39–56. https://doi.org/10.1016/0009-3084(94)90173-2. https://linkinghub.elsevier.com/retrieve/pii/0009308494901732.

11. Gomis Perez, C., N. R. Dudzinski, …, E. Karatekin. 2022. Rapid propagation of membrane tension at retinal bipolar neuron presynaptic terminals. *Sci. Adv.* 8:eabl4411. https://www.science.org/doi/10.1126/sciadv.abl4411.

12. Sadeghi, M., and F. Noé. 2020. Large-scale simulation of biomembranes incorporating realistic kinetics into coarse-grained models. *Nat. Commun.* 11:2951. https://doi.org/10.1038/s41467-020-16424-0. http://www.nature.com/articles/s41467-020-16424-0.

13. Putzel, G. G., M. J. Uline, …, M. Schick. 2011. Interleaflet coupling and domain registry in phase-separated lipid bilayers. *Biophys. J.* 100:996–1004. https://doi.org/10.1016/j.bpj.2011.01.021. https://linkinghub.elsevier.com/retrieve/pii/S0006349511000671.

14. Heberle, F. A., D. Marquardt, …, G. Pabst. 2016. Subnanometer structure of an asymmetric model membrane: interleaflet coupling influences domain properties. *Langmuir.* 32:5195–5200. https://pubs.acs.org/doi/10.1021/acs.langmuir.5b04562.

15. Blosser, M. C., A. Honerkamp-Smith, …, S. L. Keller. 2015. Transbilayer colocalization of lipid domains explained via measurement of strong coupling parameters. *Biophys. J.* 109:2317–2327. https://doi.org/10.1016/j.bpj.2015.10.031. https://linkinghub.elsevier.com/retrieve/pii/S0006349515011066.

16. Stottrup, B. L., S. L. Veatch, and S. L. Keller. 2004. Nonequilibrium behavior in supported lipid membranes containing cholesterol. *Biophys. J.* 86:2942–2950. https://doi.org/10.1016/s0006-3495(04)74345-3. https://linkinghub.elsevier.com/retrieve/pii/S0006349504743453.

17. Garg, S., J. Rühe, …, C. A. Naumann. 2007. Domain registration in raft-mimicking lipid mixtures studied using polymer-tethered lipid bilayers. *Biophys. J.* 92:1263–1270. https://doi.org/10.1529/biophysj.106.091082. https://linkinghub.elsevier.com/retrieve/pii/S0006349507709372.

18. Collins, M. D., and S. L. Keller. 2008. Tuning lipid mixtures to induce or suppress domain formation across leaflets of unsupported asymmetric bilayers. *Proc. Natl. Acad. Sci. USA.* 105:124–128. http://www.pnas.org/cgi/doi/10.1073/pnas.0702970105.

19. Nickels, J. D., J. C. Smith, and X. Cheng. 2015. Lateral organization, bilayer asymmetry, and inter-leaflet coupling of biological membranes. *Chem. Phys. Lipids.* 192:87–99. https://doi.org/10.1016/j.chemphyslip.2015.07.012. https://linkinghub.elsevier.com/retrieve/pii/S0009308415300177.

20. Raphael, R., and R. Waugh. 1996. Accelerated interleaflet transport of phosphatidylcholine molecules in membranes under deformation. *Biophys. J.* 71:1374–1388. https://doi.org/10.1016/s0006-3495(96)79340-2. https://linkinghub.elsevier.com/retrieve/pii/S0006349596793402.

21. Bitbol, A.-F., J.-B. Fournier, …, N. Puff. 2011. Dynamical membrane curvature instability controlled by intermonolayer friction. *J. Phys. Condens. Matter.* 23:284102. https://doi.org/10.1088/0953-8984/23/28/284102. https://iopscience.iop.org/article/10.1088/0953-8984/23/28/284102.

22. Pott, T., and P. Méléard. 2002. The dynamics of vesicle thermal fluctuations is controlled by intermonolayer friction. *Europhys. Lett.* 59:87–93. https://doi.org/10.1209/epl/i2002-00163-6. https://iopscience.iop.org/article/10.1209/epl/i2002-00163-6.

23. Merkel, R., E. Sackmann, and E. Evans. 1989. Molecular friction and epitactic coupling between monolayers in supported bilayers. *J. Phys.* 50:1535–1555. https://doi.org/10.1051/jphys:0198900500120153500. http://www.edpsciences.org/10.1051/jphys:0198900500120153500.

24. Tabaei, S. R., J. J. J. Gillissen, and N.-J. Cho. 2016. Probing membrane viscosity and interleaflet friction of supported lipid bilayers by tracking electrostatically adsorbed, nano-sized vesicles. *Small.* 12:6338–6344. https://onlinelibrary.wiley.com/doi/10.1002/smll.201601561.

25. Schoch, R. L., I. Barel, …, G. Haran. 2018. Lipid diffusion in the distal and proximal leaflets of supported lipid bilayer membranes studied by

single particle tracking. *J. Chem. Phys.* 148:123333. http://aip.scitation.org/doi/10.1063/1.5010341.

26. Pfeiffer, W., S. König, …, E. Sackmann. 1993. Neutron spin echo study of membrane undulations in lipid multibilayers. *Europhys. Lett.* 23:457–462. https://doi.org/10.1209/0295-5075/23/6/013. https://iopscience.iop.org/article/10.1209/0295-5075/23/6/013.

27. Jönsson, P., J. P. Beech, …, F. Höök. 2009. Shear-driven motion of supported lipid bilayers in microfluidic channels. *J. Am. Chem. Soc.* 131:5294–5297. https://pubs.acs.org/doi/10.1021/ja809987b.

28. Horner, A., S. A. Akimov, and P. Pohl. 2013. Long and short lipid molecules experience the same interleaflet drag in lipid bilayers. *Phys. Rev. Lett.* 110:268101.

29. Przybylo, M., J. Sýkora, …, M. Hof. 2006. Lipid diffusion in giant unilamellar vesicles is more than 2 times faster than in supported phospholipid bilayers under identical conditions. *Langmuir.* 22:9096–9099. https://pubs.acs.org/doi/10.1021/la061934p.

30. Zhang, L., and S. Granick. 2005. Lipid diffusion compared in outer and inner leaflets of planar supported bilayers. *J. Chem. Phys.* 123:211104. http://aip.scitation.org/doi/10.1063/1.2138699.

31. Hetzer, M., S. Heinz, …, T. M. Bayerl. 1998. Asymmetric molecular friction in supported phospholipid bilayers revealed by NMR measurements of lipid diffusion. *Langmuir.* 14:982–984. https://pubs.acs.org/doi/10.1021/la9712810.

32. Scomparin, C., S. Lecuyer, …, B. Tinland. 2009. Diffusion in supported lipid bilayers: influence of substrate and preparation technique on the internal dynamics. *Eur. Phys. J. E.* 28:211–220. https://doi.org/10.1140/epje/i2008-10407-3. http://link.springer.com/10.1140/epje/i2008-10407-3.

33. Macháň, R., and M. Hof. 2010. Lipid diffusion in planar membranes investigated by fluorescence correlation spectroscopy. *Biochim. Biophys. Acta.* 1798:1377–1391. https://linkinghub.elsevier.com/retrieve/pii/S0005273610000544.

34. den Otter, W., and S. Shkulipa. 2007. Intermonolayer friction and surface shear viscosity of lipid bilayer membranes. *Biophys. J.* 93:423–433. https://doi.org/10.1529/biophysj.107.105395. https://linkinghub.elsevier.com/retrieve/pii/S0006349507712961.

35. Zgorski, A., R. W. Pastor, and E. Lyman. 2019. Surface shear viscosity and interleaflet friction from nonequilibrium simulations of lipid bilayers. *J. Chem. Theor. Comput.* 15:6471–6481. https://pubs.acs.org/doi/10.1021/acs.jctc.9b00683.

36. Jönsson, P., J. P. Beech, …, F. Höök. 2009. Mechanical behavior of a supported lipid bilayer under external shear forces. *Langmuir.* 25:6279–6286. https://pubs.acs.org/doi/10.1021/la8042268.

37. Angelova, M. I., S. Soléau, …, P. Bothorel. 1992. *In* Preparation of Giant Vesicles by External AC Electric Fields. Kinetics and Applications. Steinkopff, Darmstadt, pp. 127–131, Progress in Colloid & Polymer Science. http://link.springer.com/10.1007/BFb0116295.

38. Jönsson, P., A. Gunnarsson, and F. Höök. 2011. Accumulation and separation of membrane-bound proteins using hydrodynamic forces. *Anal. Chem.* 83:604–611. https://pubs.acs.org/doi/10.1021/ac102979b.

39. Chada, N., K. P. Sigdel, …, G. M. King. 2015. Glass is a viable substrate for precision force microscopy of membrane proteins. *Sci. Rep.* 5:12550. https://doi.org/10.1038/srep12550. http://www.nature.com/articles/srep12550.

40. Bruus, H. 2008. Theoretical Microfluidics. Oxford University Press.

41. Gervais, T., J. El-Ali, …, K. F. Jensen. 2006. Flow-induced deformation of shallow microfluidic channels. *Lab Chip.* 6:500. https://doi.org/10.1039/b513524a. http://xlink.rsc.org/?DOI=b513524a.

42. Schindelin, J., I. Arganda-Carreras, …, A. Cardona. 2012. Fiji: an open-source platform for biological-image analysis. *Nat. Methods.* 9:676–682. https://doi.org/10.1038/nmeth.2019.

43. Jönsson, P., and F. Höök. 2011. Effects of surface pressure and internal friction on the dynamics of shear-driven supported lipid bilayers. *Langmuir.* 27:1430–1439. https://pubs.acs.org/doi/10.1021/la103959w.

44. Marquardt, D., F. A. Heberle, …, J. Katsaras. 2016. Lipid bilayer thickness determines cholesterol's location in model membranes. *Soft Matter.* 12:9417–9428. https://doi.org/10.1039/c6sm01777k. http://xlink.rsc.org/?DOI=C6SM01777K.

45. Bahrami, M., M. M. Yovanovich, and J. R. Culham. 2006. Pressure drop of fully-developed, laminar flow in microchannels of arbitrary cross-section 12. *J. Fluids Eng.* 128:632–637. https://doi.org/10.1115/1.2175171.

46. Jönsson, P., and B. Jönsson. 2015. Hydrodynamic forces on macromolecules protruding from lipid bilayers due to external liquid flows. *Langmuir.* 31:12708–12718. https://pubs.acs.org/doi/10.1021/acs.langmuir.5b03421.

47. Charrier, A., and F. Thibaudau. 2005. Main phase transitions in supported lipid single-bilayer. *Biophys. J.* 89:1094–1101. https://doi.org/10.1529/biophysj.105.062463. https://linkinghub.elsevier.com/retrieve/pii/S0006349505727570.

48. Gunderson, R. S., and A. R. Honerkamp-Smith. 2018. Liquid-liquid phase transition temperatures increase when lipid bilayers are supported on glass. *Biochim. Biophys. Acta.* 1860:1965–1971. https://linkinghub.elsevier.com/retrieve/pii/S000527361830141X.

49. Butler, P. J., G. Norwich, …, S. Chien. 2001. Shear stress induces a time- and position-dependent increase in endothelial cell membrane fluidity. *Am. J. Physiol. Cell Physiol.* 280:C962–C969. https://www.physiology.org/doi/10.1152/ajpcell.2001.280.4.C962.

50. Yamamoto, K., and J. Ando. 2013. Endothelial cell and model membranes respond to shear stress by rapidly decreasing the order of their lipid phases. *J. Cell Sci.* 126:1227–1234. http://jcs.biologists.org/cgi/doi/10.1242/jcs.119628.

51. Kumaraswamy, G., R. K. Verma, and J. A. Kornfield. 1999. Novel. Novel flow apparatus for investigating shear-enhanced crystallization and structure development in semicrystalline polymers. *Rev. Sci. Instrum.* 70:2097–2104. https://doi.org/10.1063/1.1149720.

52. Winter, R. 2001. Effects of hydrostatic pressure on lipid and surfactant phases. *Curr. Opin. Colloid Interface Sci.* 6:303–312. https://doi.org/10.1016/s1359-0294(01)00092-9. https://linkinghub.elsevier.com/retrieve/pii/S1359029401000929.

53. Alessandrini, A., and P. Facci. 2014. Phase transitions in supported lipid bilayers studied by AFM. *Soft Matter.* 10:7145–7164. https://doi.org/10.1039/c4sm01104j. http://xlink.rsc.org/?DOI=C4SM01104J.

54. Uline, M. J., M. Schick, and I. Szleifer. 2012. Phase behavior of lipid bilayers under tension. *Biophys. J.* 102:517–522. https://doi.org/10.1016/j.bpj.2011.12.050. https://linkinghub.elsevier.com/retrieve/pii/S0006349512000409.

55. Portet, T., S. E. Gordon, …, S. L. Keller. 2012. Increasing membrane tension decreases miscibility temperatures; an experimental demonstration via micropipette aspiration. *Biophys. J.* 103:L35–L37. https://doi.org/10.1016/j.bpj.2012.08.061. https://linkinghub.elsevier.com/retrieve/pii/S0006349512010314.

56. Chen, D., and M. M. Santore. 2014. Large effect of membrane tension on the fluid–solid phase transitions of two-component phosphatidylcholine vesicles. *Proc. Natl. Acad. Sci. USA.* 111:179–184. https://pnas.org/doi/full/10.1073/pnas.1314993111.

57. Chakraborty, S., M. Doktorova, …, R. Ashkar. 2020. How cholesterol stiffens unsaturated lipid membranes. *Proc. Natl. Acad. Sci. USA.* 117:21896–21905. https://pnas.org/doi/full/10.1073/pnas.2004807117.

58. Pan, J., S. Tristram-Nagle, and J. F. Nagle. 2009. Effect of cholesterol on structural and mechanical properties of membranes depends on lipid chain saturation. *Phys. Rev. E.* 80:021931. https://link.aps.org/doi/10.1103/PhysRevE.80.021931.

59. Nagle, J. F., E. A. Evans, …, R. Dimova. 2021. A needless but interesting controversy. *Proc. Natl. Acad. Sci. USA.* 118. e2025011118. https://pnas.org/doi/full/10.1073/pnas.2025011118.

60. Ashkar, R., M. Doktorova, …, M. F. Brown. 2021. Reply to Nagle et al.: the universal stiffening effects of cholesterol on lipid membranes. *Proc. Natl. Acad. Sci. USA.* 118. e2102845118. https://pnas.org/doi/full/10.1073/pnas.2102845118.